IEEE Robotics and Automation Letters (RAL) paper presented at the
2020 IEEE/RSJ International Conference on Intelligent Robots and Systems (IROS)
October 25-29, 2020, Las Vegas, NV, USA (Virtual)

Evaluation of the response characteristics of on-chip gel actuators for various single cell manipulations

Hiroki Wada[1], Yuha Koike[2], Yoshiyuki Yokoyama[3] and Takeshi Hayakawa[1]

Abstract— **On-chip gel actuators are potential candidates for single cell manipulation because they can realize low-invasive manipulation of various cells. We propose an on-chip gel actuator driven by light irradiation. By patterning the gel actuator with light absorber, we can control the temperature of the actuator and drive it. The proposed drive method can realize highly localized temperature control of the gel actuator and can be applied to mass integration of on-chip gel actuators. In this study, we evaluate the heat conduction of the actuator during driving and its response characteristics as a function of various design parameters. We theoretically and experimentally evaluate the response characteristics and confirm that the response characteristics can be changed by altering the size of the light absorber. Furthermore, we show some examples of cell manipulation including trapping, transport, and sorting with various sizes of light absorber. Finally, we show proof of concept for the application of the proposed drive method for massive integration of on-chip gel actuators.**

I. INTRODUCTION

Recently, the demands on single cell analysis technologies have been increasing owing to their importance in cell biology, medicine, and commercial applications such as in bioindustries and personalized medicine [1]–[4]. Single cell manipulation techniques are essential for achieving single cell analysis. Mechanical micromanipulators are among the most popular instruments for single cell manipulation and single cell analysis [5], [6]. Generally, mechanical micromanipulators have dual 3-DOF manipulators with high positioning accuracy. Various end effectors such as glass capillaries and electrodes can be attached to these manipulators. Thus, mechanical manipulators can realize various single cell manipulations such as fixing, transportation, cutting, pushing, or injecting DNA or biological reagents into target cells. Because of this flexibility, mechanical micromanipulators are widely used for practical single cell manipulation and analysis.

Another example of a single cell analysis technique is fluorescence-activated cell sorting (FACS), which is a current de facto standard method for single cell analysis in the field of cell biology [7], [8]. FACS flows target cells into a narrow fluidic channel to restrict their movement in 1-DOF and transport them to the analyzer. After analyzing the target cells based on their fluorescence, each analyzed cell is encapsulated in a microdroplet. These droplets are manipulated with electrostatic force and dispensed into cell culture chambers. Thus, FACS can separate single cells according to biological information acquired from the fluorescent signal, using both fluidic force and electrostatic force. As explained above, mechanical micromanipulators and FACS are powerful tools for single cell analysis. However, mechanical micromanipulators are generally used as part of manual operations by experienced operators, which leads to low-repeatability and low-throughput processes. Although FACS is suitable for high-throughput single cell analysis, it is limited to sorting cells with fluorescent signals. Additionally, the capital cost for these techniques is high.

Microfluidic chips are a new potential platform for single cell analysis. Microfluidic chips consist of microfluidic channels or chambers integrated with on-chip sensors or actuators and are fabricated using microfabrication techniques. The small spaces on microfluidic chips reduce the degrees of freedom of target cells, enabling cell manipulation with high accuracy and high throughput. Furthermore, microfabrication is suitable for mass production, allowing microfluidic chips to be disposable, which is preferable for biomedical applications. Therefore, various microfluidic chips have been proposed for single cell analysis using various on-chip single cell manipulation functions, such as trapping [9], patterning [10], transport [11], sorting [12], and rotation [13].

On-chip cell manipulation methods are classified as non-contact or contact methods. Non-contact cell manipulation uses external forces, such as optical [14], magnetic [15], electrical [16], or acoustic [17] forces to manipulate cells without physical contact with the target cells. The non-contact characteristics of these methods reduce the risks of cell damage as a result of physical contact and undesired cell adhesion. However, the manipulation forces of these methods are weak and independent actuation of large numbers of cells is difficult because the manipulation is driven by applying external fields from outside the chip. Therefore, non-contact cell manipulation is generally suitable for applications requiring low invasiveness with simple cell manipulations such as cell culture [18], patterning [10], or focusing [19]. In contrast, contact cell manipulation uses microstructures [20], microtools [21], or microrobots [22] for cell manipulation through physical contact with target cells. Although contact manipulation methods can apply greater force than non-contact methods, cell damage and adhesion are essentially inevitable. Thus, contact manipulation is suitable for high-throughput applications requiring large forces or complex

*This work was supported by a Chuo University Personal Research Grant and a Grant for Special Research

[1]H. Wada, and T. Hayakawa are with Department of Precision Engineering, Undergraduate School of Science and Engineering, Chuo University, Tokyo, Japan hayaka-t@mech.chuo-u.ac.jp

[2]Y. Koike is with Department of Precision Mechanics, Graduate School of Science and Engineering, Chuo University, Tokyo, Japan

[3]Y. Yokoyama is with Toyama Industrial Technology Research and Development Center, Toyama, Japan

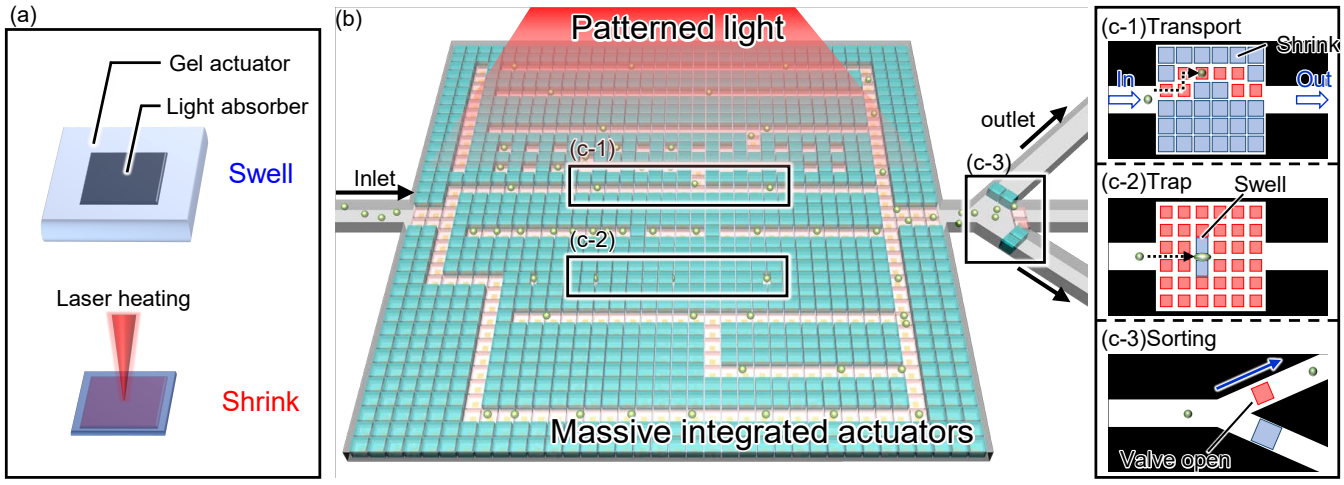

Fig. 1. Concept of massive integrated gel actuators for various cell manipulations: (a) principle of the light irradiation-based drive method, (b) schematic overview of the device used for various cell manipulations, (c) examples of cell manipulations using the device.

manipulation such as mechanical cell stimulation [23] and cell stiffness measurement [24].

To overcome these limitations, low-invasive contact cell manipulation using on-chip gel actuators has been proposed [25]. Poly(N-isopropylacrylamide) (PNIPAAm), which is a temperature responsive hydrogel, is commonly used as a material for on-chip gel actuators [26]–[29]. PNIPAAm shrinks at temperatures higher than the lower critical solution temperature (LCST) ($\gtrsim$ 32 °C) and swells at temperatures lower than the LCST ($\lesssim$ 32 °C). These volume changes can be used as an actuator. Because hydrogels such as PNIPAAm have similar softness to cells ($\approx$ 100 kPa), as well as hydrophilic surface characteristics, on-chip gel actuators can prevent both physical damage and adhesion of cells at actuator and target cell contact points.

Previously, we proposed driving on-chip gel actuators using light irradiation [30]. In this method, gel actuators were patterned with light absorber as shown in Fig. 1 (a). As a result, the actuators could be driven by irradiating the absorber, which controlled the temperature of the actuator. In our previous work, we succeeded in driving on-chip gel actuators with the proposed method. Furthermore, we showed that the proposed method can realize independent driving of a single actuator among mass integrated actuators. In this study, we evaluate the response characteristics of actuators with various sizes of light absorber driven by light irradiation. We theoretically evaluate heat conduction from light absorbers to gel actuators and the surrounding environment during shrinking and swelling, and discuss differences in the response characteristics between various sizes of light absorber according to the theoretical calculations. Furthermore, we also evaluate the response characteristics experimentally and compare the findings with the theoretical results. Finally, we show some examples of cell manipulation with integrated on-chip gel actuators using the proposed drive method.

II. METHOD

A. Concept of light-driven on-chip gel actuator cell manipulation

The proposed gel actuator drive method uses light irradiation to control the temperature of the actuators. The gel actuators are patterned on a microfluidic chip with light absorbers, as shown in Fig. 1 (a). Because this drive method can realize highly localized heating of the gel actuator, as shown in our previous work [30], we can integrate a large number of gel actuators on a chip and selectively drive particular actuators by irradiating with patterned light as shown in Fig.1 (b). Therefore, the proposed drive method can be used for various cell manipulations such as transport via a given flow path, trapping at multiple positions, or sorting of single cells, as shown in Fig.1 (c).

B. Fabrication process

The on-chip gel actuators and light absorbers were fabricated by using microfabrication processes. The detailed fabrication process is as follows.

(a) deposition of chromium (Cr) layer on the glass substrate
(b) OFPR patterning (OFPR-800 LB 200cp, Tokyo Ohka Kogyo Corporation, Kanagawa, Japan) on the Cr as an etching mask
(c) etching the Cr and removal of OFPR
(d) spin coating PNIPAAm on the light absorbers
(e) patterning the PNIPAAm
(f) bonding polydimethylsiloxane (PDMS) (silpot 184, Dow Corning, Michigan, America) as a microfluidic channel

The PDMS microchannel was molded by patterned SU-8 (SU-8 3025, Nipon Kayaku Co. Ltd., Tokyo, Japan). To pattern PNIPAAm, we used photo-processable PNIPAAm (Bioresist, Nissan Chemical Corporation, Tokyo, Japan).

C. Experimental system

A schematic diagram of the light irradiation system is shown in Fig. 2 (a). We used a digital mirror device (DMD) (Keynote Photonics, LC4500-RGB-EKT) to generate an arbitrary light pattern. DMDs are commonly used for generating light patterns for example in commercially available projectors and light exposure systems on microscopes [31]–[33]. We used a DMD for infrared (IR) light and its resolution was 912×1140 pixels. As a light source we used an IR laser (SP-020P-AHS-S, SPI Lasers, max. power: 20 W). The wavelength of the IR laser was 1064 nm, which was selected because the absorbance of water at this wavelength is low. Thus, this wavelength minimizes cell damage and unintended heating of the hydrogel actuators. We focused the IR laser with an objective lens (LMPlan N 10x/0.30Na IR and LCPlan N 20x/0.45Na IR, Olympus, Tokyo, Japan) and acquired microscope images using a CCD camera (GS3-U3-32S4C-C, FLIR Systems Japan K.K., Tokyo, Japan). A dichroic mirror (86-694, Edmund Optics, Barrington, USA, cutoff wavelength: 950 nm) was used to obtain visible light from the light source. A photograph of the experimental system is shown in Fig.2 (b).

III. Evaluation of the Response Characteristics of the Actuator

A. Theoretical analysis of heat transfer

To optimize the design of the actuator and light absorber, we performed theoretical analysis of heat transfer through the gel actuator, light absorber, glass substrate and surrounding environment. In our model we considered one square actuator with length l_{gel} and thickness τ_{gel} on a glass substrate, as shown in Fig. 3 (a). Similarly, a square light absorber with length l_{Cr} and thickness τ_{Cr} were put on the bottom of the actuator. The Biot number B_i, which is a dimensionless parameter for heat conduction, is written as follows.

$$B_i = \frac{hL}{\lambda} \tag{1}$$

Where, h is the heat transfer coefficient, L is the characteristic length, and λ is the thermal conductivity. The Biot number indicates the ratio of heat conduction inside a body and at the surface of the body. In our model, we assume these values to be $h \approx 100-1000$ [W/(m^2·K)], $L = 100 \times 10^{-6}$ [m] and $\lambda = 0.62$ [W/(m·K)]. The values of h are common values for the heat transfer coefficient of the surrounding liquid. L is the order of size of the fabricated gel actuators and λ is the thermal conductivity of water because most of the gel actuator volume consists of water. Thus, the order of the Biot number is $B_i \approx 0.001 - 0.01$ and it can be assumed to be less than 0.1. This means that the heat conduction inside the body is much greater than the heat conduction at the surface. Thus, we used the lumped capacitance model, which assumes the temperature distribution in the solid is uniform. We therefore assumed that the heat conduction inside the actuator and light absorber is much faster than the heat conduction at the surface and each material has uniform temperature. Hereafter, we consider two states of

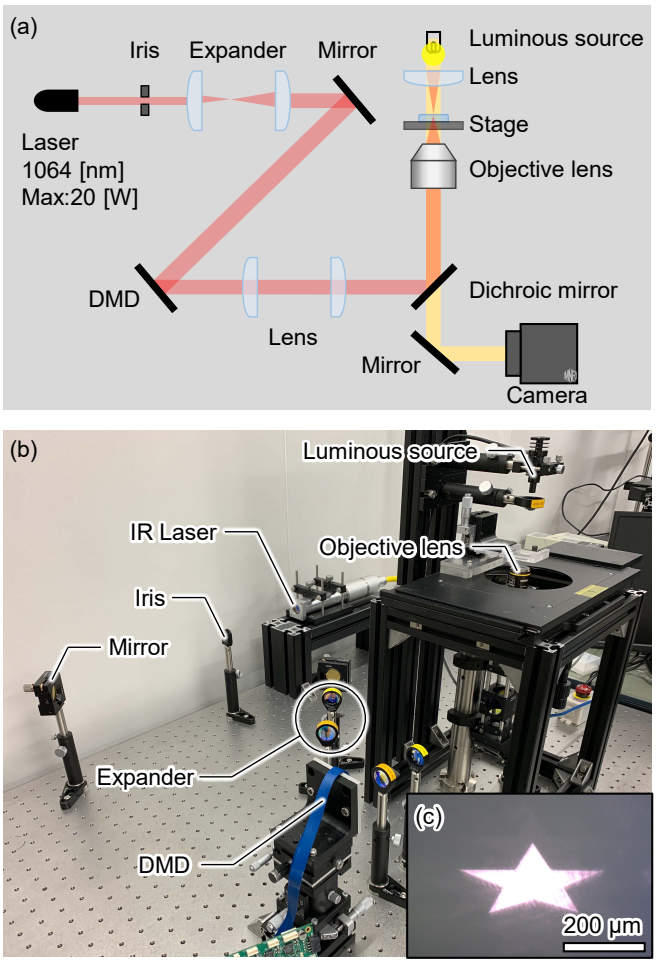

Fig. 2. Experimental system. (a) Schematic diagram of the light irradiation system, (b) photograph of the system, (c) microscope image of irradiated patterned light.

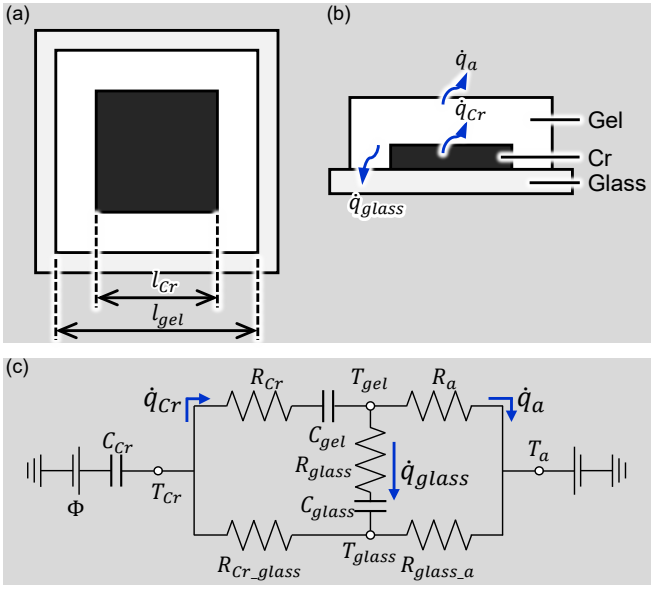

Fig. 3. Schematic diagram of the thermal conductivity model and an analogous circuit for the model. (a) Top view and (b) side view of the system, (c) equivalent circuit for the heat transfer model.

heat conduction. One is the absorption of heat by an actuator, which corresponds to the phase transition from the swollen state to the shrunken state. The other is heat dissipation, which corresponds to the phase transition from the shrunken state to the swollen state.

First, we explain the absorption of heat. By considering energy conservation per unit time, the dominant equation for the temperature of the actuator T is as follows.

$$C_{gel}\rho_{gel}V_{gel}\frac{dT}{dt} = \dot{q}_{Cr} - \dot{q}_a - \dot{q}_{glass} \tag{2}$$

Where, C_{gel}, ρ_{gel}, and V_{gel} are the heat capacity, density, and volume of the gel actuator, respectively. $\dot{q}_{Cr}, \dot{q}_a, \dot{q}_{glass}$ are heat fluxes, from Cr to the gel actuator and from the gel actuator to the environment and glass substrate, respectively, as shown in Fig.3 (b).

In addition, we can obtain the equations for the heat fluxes on the righthand side of eq. (2) by taking into account Newton's cooling law and the energy conservation in Cr, as follows.

$$\dot{q}_{Cr} = \varepsilon_{Cr}A_{Cr}I_u - C_{Cr}\rho_{Cr}V_{Cr}\Delta_{Cr} \tag{3}$$
$$\dot{q}_a = A_{gel}h_{gel}(T - T_a) \tag{4}$$
$$\dot{q}_{glass} = A_{glass}h_{glass}(T - Ta) \tag{5}$$

Where, ε_{Cr}, I_u, and Δ_{Cr} are the laser absorption rate of Cr, laser power density, and the rate of temperature change per unit time at Cr, respectively. A, and h are the surface area and heat transfer coefficient of Cr, gel, and glass as represented by subscripts. To solve these equations, we assume that the temperature of Cr linearly increased with time. In this case, the solution of the differential eq. (2) under the initial condition; $T = T_a$ at $t = 0$ is described as follows.

$$T(t) = T_a + \frac{\dot{q}_{Cr}}{A_{gel}h_{gel} + A_{glass}h_{glass}} \times \left[1 - \exp\left(-\frac{A_{gel}h_{gel} + A_{glass}h_{glass}}{C_{gel}\rho_{gel}V_{gel}}t\right)\right] \tag{6}$$

To estimate the effect of light absorber size on response time, we define the dimensionless parameter $l = l_{Cr}/l_{gel}$ as a ratio of the length of the gel actuator and light absorber. By using this l, we can rewrite equation (6) to indicate $t(l)$ as a function of time t, as follows.

$$t(l) = \frac{P_{gel}}{h_{gel}\left(2 + 4\frac{\tau_{gel}}{l_{gel}}\right) + h_{glass}(1 - l^2)} \times \ln\left|\frac{\dot{q}_{Cr}}{\dot{q}_{Cr} - h_{gel}\left(2 + 4\frac{\tau_{gel}}{l_{gel}}\right) + h_{glass}(1 - l^2)(T - T_a)}\right| \tag{7}$$

Where, P_{gel} is summary constant related to the actuator and expressed, as follows.

$$P_{gel} = C_{gel}\rho_{gel}\tau_{gel} \tag{8}$$

Second, we performed the analysis of the heat dissipation. Similarly to the heat absorption in eq. (2), the dominant equation at the actuator can be obtained by considering the energy conservation per unit time about the actuator and is expressed as follows.

$$C_{gel}\rho_{gel}V_{gel}\frac{dT}{dt} = -\dot{q}_{Cr} - \dot{q}_a - \dot{q}_{glass} \tag{9}$$

Here we note that differences in the signs on the righthand side of the equation indicate differences in the direction of heat conduction. Moreover, each term on the righthand side is described as follows with Newton's cooling law.

$$\dot{q}_{Cr} = A_{Cr}h_{Cr}(T - T_{Cr}) \tag{10}$$
$$\dot{q}_a = A_{gel}h_{gel}(T - T_a) \tag{11}$$
$$\dot{q}_{glass} = A_{glass}h_{glass}(T - T_a) \tag{12}$$

In this case, we assume that the initial temperature of the Cr and the gel actuator is same at 60 °C. Under these assumptions, the solution of the differential equation (9) is expressed as follows given that when $t = 0, T = T_0$.

$$T(t) = \left(\frac{1}{R_{gel}} + \frac{1}{R_{glass}}\right)RT_a + \frac{R}{R_{Cr}}(T_{Crini} - \Delta_{Cr}t) + \frac{R^2}{R_{Cr}}P_{gel}\Delta_{Cr} + Ce^{-\frac{1}{RP_{gel}}t} \tag{13}$$

Where, R are the thermal resistances of the materials represented by the subscripts and no subscript represents the sum of all of the resistances. In addition, C is the integration constant. The resistances of each substance are expressed as

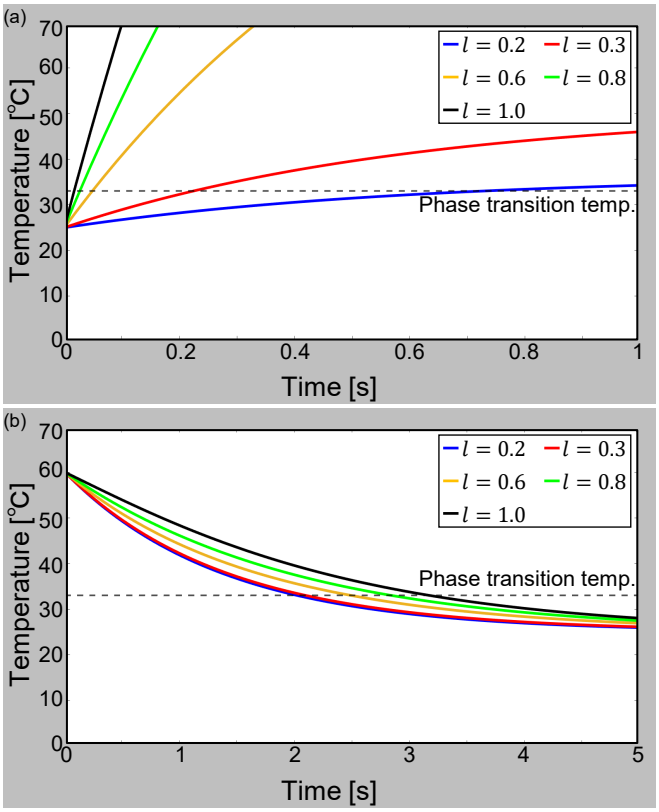

Fig. 4. Analytical results for the temperature change of an actuator with different size parameters (l = 0.2, 0.3, 0.6, 0.8, and 1.0) of light absorber. (a) shrunken state, (b) swollen state.

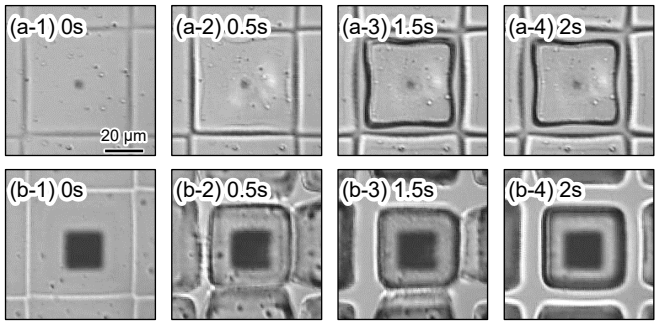

Fig. 5. Microscope images of actuator shrinking with different sizes of light absorber. (a) $l = 0.2$, (b) $l = 0.6$. The length of the gel actuator is 50 μm for both cases. The length of the light absorber is 10 μm for (a) and 30 μm for (b).

the function of l, as follows.

$$1/R_{gel} = \left(2 + 4\frac{\tau_{gel}}{l_{gel}}\right) h_{gel} \tag{14}$$

$$1/R_{Cr} = \left(2l^2 + 4\frac{\tau_{gel}}{l_{gel}}\right) h_{Cr} \tag{15}$$

$$1/R_{glass} = \left(1 - l^2\right) h_{glass} \tag{16}$$

The theoretical values of $T(t)$ in the cases of shrinking and swelling are shown in Fig.4 (a) and (b), respectively. Hereafter, we evaluate the response characteristics of the actuator using these plots.

B. Experimental evaluation of the response time and comparison with the theoretical results

To confirm the response characteristics of actuators with various sizes of light absorber, we evaluated the displacements experimentally. The typical shrinking response of the actuator is shown in Fig.5. As we can see in Fig. 5, actuators with larger light absorbers shrink faster than actuators with smaller light absorbers.

To quantitatively evaluate the response time of the actuators, their displacements were measured using microscope images and the results are shown in Fig. 6. Fig. 6 shows that shrinking of the actuators was faster than swelling of the actuators, similarly to trends in the temperature responses of the theoretical results in Figs. 4. Here, we note that there was a different trend in the case of $l = 0.6$, $l = 0.8$, and $l = 1.0$ in Fig. 6 (b). In these cases, the actuators with larger light absorber have slightly better response characteristics during swelling. The reason for this different trend is thought to be the balance of the initial high-temperature area and the thermal transfer via the light absorber. Commonly, the light absorber is a high-temperature source under the initial conditions in the system during swelling. This is why smaller light absorbers have good response characteristics for swelling, as shown in Fig. 4 (b). However, the light absorber has much higher thermal conductivity than other materials in the system, such as glass or water. Thus, with some values of actuator and light absorber size there may be the opposite trend that a larger light absorber has better characteristics for example in the cases of $l = 0.6$, 0.8 and 1.0 in Fig. 6 (b).

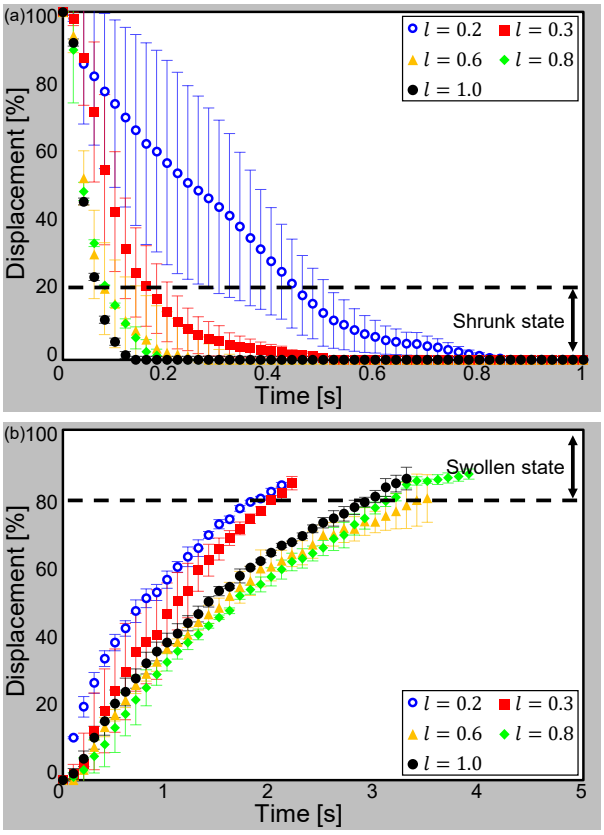

Fig. 6. Experimental results for the response evaluation of the actuator. (a) Shrunken state, (b) swollen state.

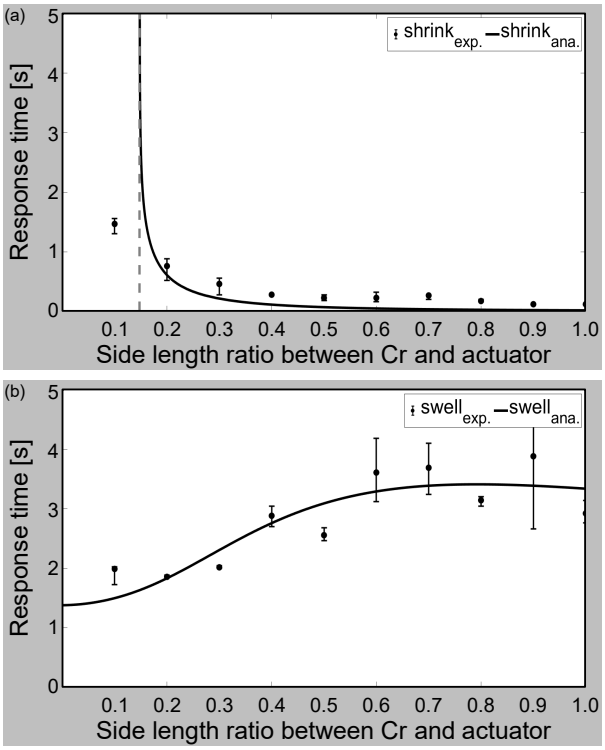

Fig. 7. Comparison of the theoretical and experimental response time results. The solid line and dot plots represent the theoretical and experimental data, respectively. (a) Shrunken state, (b) swollen state.

Although Fig. 4 shows theoretical results for actuator temperature and Fig. 6 shows experimental results for the actuator displacement, the relationship between temperature and the gel actuator was previously evaluated in ref. [28]. Practically, the direct measurement of actuator temperature is difficult. Therefore, we compared the theoretical results for temperature and experimental results for displacement to evaluate the response characteristics of the actuators.

To compare the experimental and theoretical results, we defined the response time as the time taken for the actuator to reach the phase transition temperature (32 °C) in the case of both shrinking and swelling. In the case of the experimental data, we defined the response time as The time for the displacement of the actuator to become 80% of the maximum, as shown in Fig. 6.

Results of the response time for the theoretical and experimental data in the shrunken state and swollen state are shown in Fig.7 (a) and (b), respectively. The theoretical and experimental plots in Fig. 7 show good agreement, particularly in the $l = 0.2$ to $l = 1.0$ region. From Fig. 7 (a) it can be seen that a larger light absorber achieves a faster shrinking response in both the results of theoretical calculations and experimental results. In contrast, a smaller light absorber achieves a faster swelling response, Fig. 7 (b). Thus, we can design light-driven gel actuators with different response characteristics suitable for different applications. More specifically, the actuator with larger light absorber is suitable for applications with swollen initial actuator states. In these applications, a larger light absorber realizes a fast actuator response by shrinking and we show applications of this type of actuator for cell transport through an arbitrary flow path, which is demonstrated in section IV-A), and cell sorting, which is demonstrated in section IV-B). In contrast, smaller light absorbers are suitable for applications with shrunken initial actuator states. In these applications, a smaller light absorber realizes a fast actuator response by swelling. One application of this type of actuator is as a cell trap, which is demonstrated in section IV-C).

IV. Applications for Cell Manipulation

Hereafter, we show some examples of cell manipulation using actuators with various sizes of light absorber. The practical limitation for the size of the gel actuator is 20 μm based on the success rate of the fabrication processes. Therefore, in the following demonstrations, for repeatability, the sizes of the actuators used were from 50 μm to 100 μm according to purpose.

A. Cell transport with an angled channel

To demonstrate cell transport through an arbitrary flow path, we designed the 6×6 integrated actuator shown in Fig.8 (a). The size of each actuator was 50 μm in the shrunken state because the size of the target cells varied from 10 to 30 μm. The clearance between actuators was 5 μm. When all of the actuators were swollen, the main flow was stemmed by the swollen actuators. The clearance between actuators in the design was sufficiently narrow to confine the actuation direction to vertical only. Therefore, cells could pass through above the shrunk actuators, as shown in Fig. 8 (a). The actuators are normally swollen and shrink when irradiated with light. Therefore, to use this actuator array as a flow channel, a larger light absorber is suitable because large light absorbers have rapid shrink response characteristics. We determined the size of the light absorber to be 30 μm, which is equivalent to the $l = 0.6$ case we evaluated in section III.

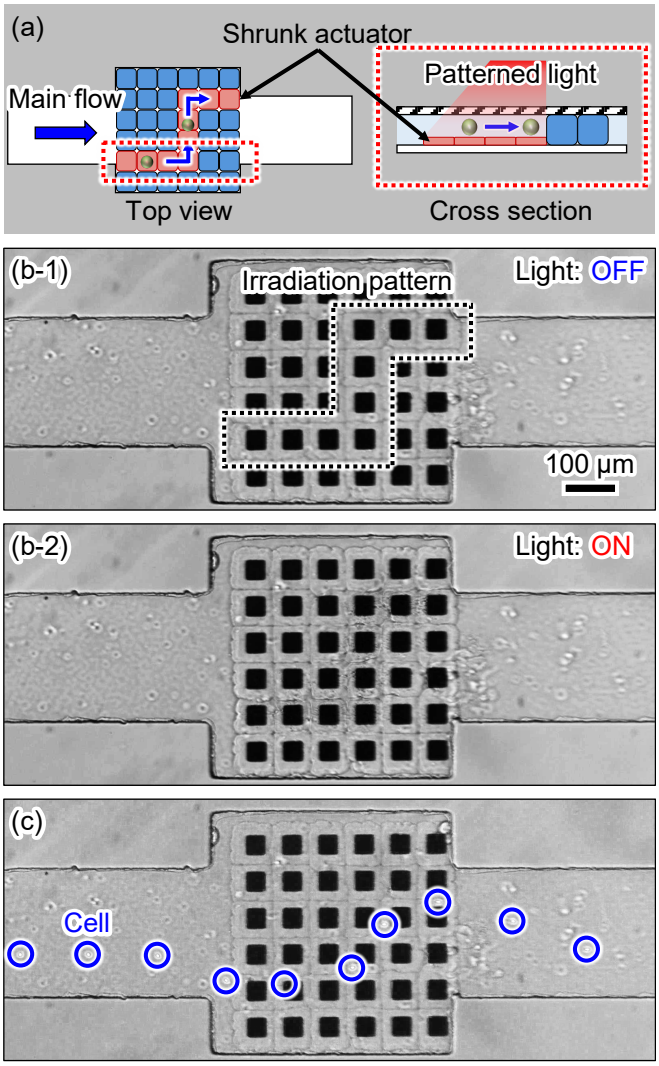

Fig. 8. Demonstration of cell transport. (a) Schematic diagram of cell transport, (b-1) gel actuator array before light irradiation, and (b-2) after light irradiation, (c) successive microscope images of cell transport. Frames were recorded every 10 ms. The lengths of the gel actuator and light absorber are 50 μm and 30 μm, respectively. These values correspond to the $l = 0.6$ case in our analysis in Section III.

In this experiment, Madin-Darby Canine Kidney cells (MDCK) were used as the target cells. We prepared a target cell suspension with a cell concentration of 5×10^5 cells/mL. The cell suspension was flowed into the channel with a flow velocity of approximately 13 mm/s. The power of the IR laser used in this experiment was approximately 100 mW/mm^2. In this experiment,

we irradiated a light pattern that had two corners, as shown in Fig. 8 (b). One target cell was moved along the flow path

made by the patterned light, as shown in Fig.8 (c). Therefore, we succeeded in transport of a target cell with given flow path by using the proposed gel actuator.

B. Cell sorting

Figure 9 shows a demonstration of cell sorting. In this experiment, we made a microchannel that branched into two and placed actuators on each microchannel. By driving an actuator placed in the channel in which we wanted flow, we were able to realize cell sorting. In other words, we used the actuator as an on-chip valve. The valve was opened when the actuator shrank. This means that these actuators are normally swollen and shrink to collect a target cell when the cells are detected. Thus, a larger light absorber with a faster shrink response is suitable for cell sorter applications.

The size of the actuator in the shrunken state was 90 μm and the size of the light absorber was 81 μm, which is equivalent to the $l = 0.9$ case we evaluated in section III. Madin-Darby Canine Kidney cells (MDCK) were used as the target cells in this experiment. We prepared a target cell suspension with a cell concentration of 5×10^5 cells/mL. The input flow rate where the actuators were not placed was 925 μm/s. The power of the IR laser used in the experiment was approximately 500 mW/mm^2. To demonstrate cell sorting, we switched the irradiation point from one channel to another channel every 5 s. As shown in Fig.9 (a) and (b), we confirmed that one cell flows to the lower branch, while the next cell flows to the upper channel. Therefore, we confirmed that the proposed gel actuator was able to work as on-chip valves and be applied to on-chip cell sorter.

C. Trapping of motile cells

Fig.10 shows schematic of cell trapping and experimental images of trapping of a motile cell. To realize cell trapping, we covered the integrated gel actuator array with a cover glass. When the array actuators shrank, motile cells could swim in the gap between the actuators, as shown in Fig. 10(a). To trap these swimming cells, we turned off the irradiation laser to swell the actuators. Then, the space between the actuators was filled by the swollen actuator and swimming cells were trapped, as shown in Fig. 10 (a). In this application, the initial state of the actuators was shrunken and the actuators swelled when the target cells were detected. Thus, actuators with smaller light absorbers, which have a faster swelling response, were suitable for this application.

We determined the size of the gel actuator to be 50 μm and that of the light absorber to be 10 μm. This size corresponds to the $l = 0.2$ case we evaluated in section III. In this experiment, the target cells were *E.gracilis* NIES-48 provided by the Microbial Culture Collection at the National Institute for Environmental Studies (NIES). The power of the IR laser was approximately 200 mW/mm^2. In this experiment, we irradiated all areas of the actuators with the laser and shrank all actuators in advance. Then, motile cells were introduced above the actuators, as shown in Fig.10 (b). The light was turned off to trap the motile cells between the swollen actuators, as shown in Fig.10 (c) and (d). When

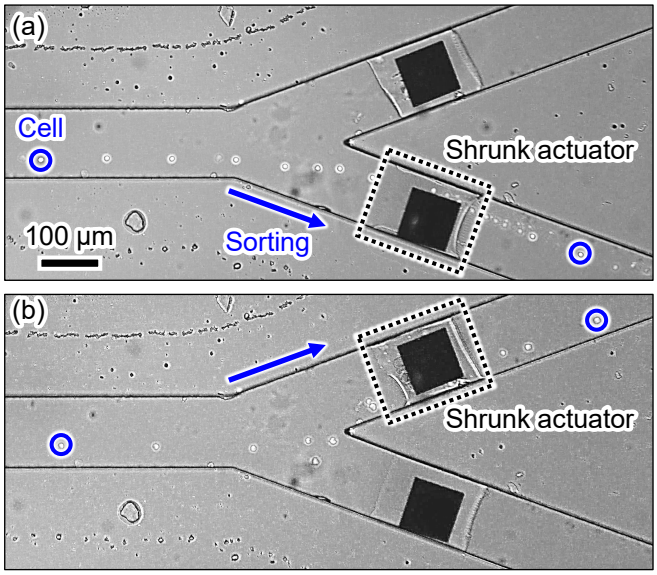

Fig. 9. Demonstration of cell sorting. Successive microscope images of (a) sorting to the bottom channel, (b) sorting to the upper channel. Images were recorded every 20 ms. The lengths of the gel actuator and light absorber were 90 μm and 81 μm, respectively. This corresponds to the $l = 0.9$ case in our analysis in Section III.

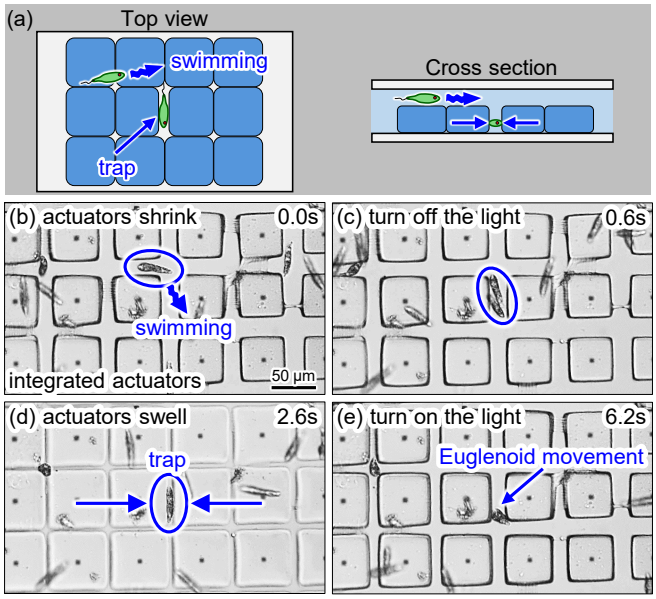

Fig. 10. Demonstration of motile cell trapping. (a) schematic image of motile cell trapping. (b) Initial state of integrated actuators. Motile cells swimming above and between the shrunk actuators (0 s), (b) the light is turned off and the actuators start to swell (0.6 s), (c) cells are trapped between the swollen actuators and cells that are not trapped swim between the actuators and glass coverslip (2.6 s), and (d) light irradiation releases the motile cells (6.2 s) The lengths of the gel actuator and light absorber were 50 μm and 10 μm, respectively. This corresponds to the $l = 0.2$ case in our analysis in Section III.

we irradiated with light again the motile cell was released, as shown in Fig.10 (e). From Fig.10 (e), we confirmed that the *Euglena* was alive and start peristaltic movement. This motion is known as euglenoid movement and is caused by mechanical stimulation. Therefore, we confirmed that the proposed actuator was able to be applied to a trap of living

cell.

V. CONCLUSION

In this study, we evaluated the response characteristics of light-driven on-chip gel actuators. We theoretically and experimentally confirmed that the response characteristics of actuators can be changed by altering the size of the light absorber. Finally, we showed some examples of cell manipulation. We conducted cell trapping, transport, and sorting using the proposed actuator. The results confirmed that the proposed light irradiation method has the potential to be applied for various cell manipulations on a chip.

ACKNOWLEDGMENT

This research was supported by a Chuo University Personal Research Grant and a Grant for Special Research. The authors also thank the Nissan Chemical Corporation for providing photo-processable PNIPAAm (Bioresist). We thank Sarah Dodds, PhD, from Edanz Group (https://en-author-services.edanzgroup.com/) for editing a draft of this manuscript.

REFERENCES

[1] F. Ye, W. Huang, and G. Guo, "Studying hematopoiesis using single-cell technologies," *Journal of hematology & oncology*, vol. 10, no. 1. 27, 2017.

[2] M. A. Walling and J. R. Shepard, "Cellular heterogeneity and live cell arrays," *Chemical Society Reviews*, vol. 40, no. 7, pp. 4049–4076, 2011.

[3] S. J. Altschuler and L. F. Wu, "Cellular heterogeneity: do differences make a difference?," *Cell*, vol. 141, no. 4, pp. 559–563, 2010.

[4] D. Wang and S. Bodovitz, "Single cell analysis: the new frontier in 'omics'," *Trends in biotechnology*, vol. 28, no. 6, pp. 281–290, 2010.

[5] K. Yanagida, H. Katayose, H. Yazawa, Y. Kimura, K. Konnai, and A. Sato, "The usefulness of a piezo-micromanipulator in intracytoplasmic sperm injection in humans," *Human Reproduction*, vol. 14, no. 2, pp. 448–453, 1999.

[6] T. Tanikawa and T. Arai, "Development of a micro-manipulation system having a two-fingered micro-hand," *IEEE Transactions on Robotics and Automation*, vol. 15, no. 1, pp. 152–162, 1999.

[7] A. Y. Fu, C. Spence, A. Scherer, F. H. Arnold, and S. R. Quake, "A microfabricated fluorescence-activated cell sorter," *Nature biotechnology*, vol. 17, no. 11, pp. 1109–1111, 1999.

[8] A. Wolff, I. R. Perch-Nielsen, U. Larsen, P. Friis, G. Goranovic, C. R. Poulsen, J. P. Kutter, and P. Telleman, "Integrating advanced functionality in a microfabricated high-throughput fluorescent-activated cell sorter," *Lab on a Chip*, vol. 3, no. 1, pp. 22–27, 2003.

[9] J. Nilsson, M. Evander, B. Hammarström, and T. Laurell, "Review of cell and particle trapping in microfluidic systems," *Analytica chimica acta*, vol. 649, no. 2, pp. 141–157, 2009.

[10] S. W. Rhee, A. M. Taylor, C. H. Tu, D. H. Cribbs, C. W. Cotman, and N. L. Jeon, "Patterned cell culture inside microfluidic devices," *Lab on a Chip*, vol. 5, no. 1, pp. 102–107, 2005.

[11] N. Pamme, "Magnetism and microfluidics," *Lab on a Chip*, vol. 6, no. 1, pp. 24–38, 2006.

[12] M. P. MacDonald, G. C. Spalding, and K. Dholakia, "Microfluidic sorting in an optical lattice," *Nature*, vol. 426, no. 6965, pp. 421–424, 2003.

[13] T. Hayakawa, S. Sakuma, and F. Arai, "On-chip 3d rotation of oocyte based on a vibration-induced local whirling flow," *Microsystems & nanoengineering*, vol. 1, no. 1, pp. 1–9, 2015.

[14] P. Y. Chiou, A. T. Ohta, and M. C. Wu, "Massively parallel manipulation of single cells and microparticles using optical images," *Nature*, vol. 436, no. 7049, pp. 370–372, 2005.

[15] C. W. Shields IV, J. L. Wang, K. A. Ohiri, E. D. Essoyan, B. B. Yellen, A. J. Armstrong, and G. P. López, "Magnetic separation of acoustically focused cancer cells from blood for magnetographic templating and analysis," *Lab on a Chip*, vol. 16, no. 19, pp. 3833–3844, 2016.

[16] C. Wu, R. Chen, Y. Liu, Z. Yu, Y. Jiang, and X. Cheng, "A planar dielectrophoresis-based chip for high-throughput cell pairing," *Lab on a Chip*, vol. 17, no. 23, pp. 4008–4014, 2017.

[17] F. Guo, Z. Mao, Y. Chen, Z. Xie, J. P. Lata, P. Li, L. Ren, J. Liu, J. Yang, M. Dao, *et al.*, "Three-dimensional manipulation of single cells using surface acoustic waves," *Proceedings of the National Academy of Sciences*, vol. 113, no. 6, pp. 1522–1527, 2016.

[18] C.-Y. Wu, D. Stoecklein, A. Kommajosula, J. Lin, K. Owsley, B. Ganapathysubramanian, and D. Di Carlo, "Shaped 3d microcarriers for adherent cell culture and analysis," *Microsystems & nanoengineering*, vol. 4, no. 1, pp. 1–9, 2018.

[19] T. E. Winkler, H. Ben-Yoav, and R. Ghodssi, "Hydrodynamic focusing for microfluidic impedance cytometry: a system integration study," *Microfluidics and Nanofluidics*, vol. 20, no. 9: 134, 2016.

[20] B. Dura, Y. Liu, and J. Voldman, "Deformability-based microfluidic cell pairing and fusion," *Lab on a Chip*, vol. 14, no. 15, pp. 2783–2790, 2014.

[21] M. Hagiwara, T. Kawahara, Y. Yamanishi, and F. Arai, "Driving method of microtool by horizontally arranged permanent magnets for single cell manipulation," *Applied Physics Letters*, vol. 97, no. 1, p. 013701, 2010.

[22] T. Kawahara, M. Sugita, M. Hagiwara, F. Arai, H. Kawano, I. Shihira-Ishikawa, and A. Miyawaki, "On-chip microrobot for investigating the response of aquatic microorganisms to mechanical stimulation," *Lab on a Chip*, vol. 13, no. 6, pp. 1070–1078, 2013.

[23] A. M. Hirsch, C. A. Rivet, B. Zhang, M. L. Kemp, and H. Lu, "Parallel multi-time point cell stimulation and lysis on-chip for studying early signaling events in t cell activation," *Lab on a Chip*, vol. 9, no. 4, pp. 536–544, 2009.

[24] K. Park, A. Mehrnezhad, E. A. Corbin, and R. Bashir, "Optomechanical measurement of the stiffness of single adherent cells," *Lab on a Chip*, vol. 15, no. 17, pp. 3460–3464, 2015.

[25] W. Lee, N. Kalashnikov, S. Mok, R. Halaoui, E. Kuzmin, A. J. Putnam, S. Takayama, M. Park, L. McCaffrey, R. Zhao, *et al.*, "Dispersible hydrogel force sensors reveal patterns of solid mechanical stress in multicellular spheroid cultures," *Nature communications*, vol. 10, no. 1, pp. 1–14, 2019.

[26] Y. Yokoyama, M. Umezaki, T. Kishimura, E. Tamiya, and Y. Takamura, "Micro-and nano-fabrication of stimulus-responsive polymer using nanoimprint lithography," *Journal of Photopolymer Science and Technology*, vol. 24, no. 1, pp. 63–70, 2011.

[27] K. Ito, S. Sakuma, Y. Yokoyama, and F. Arai, "On-chip gel-valve using photoprocessable thermoresponsive gel," *ROBOMECH Journal*, vol. 1, no. 1, pp. 1–8, 2014.

[28] T. Hayakawa, S. Sakuma, T. Fukuhara, Y. Yokoyama, and F. Arai, "A single cell extraction chip using vibration-induced whirling flow and a thermo-responsive gel pattern," *Micromachines*, vol. 5, no. 3, pp. 681–696, 2014.

[29] L. d'Eramo, B. Chollet, M. Leman, E. Martwong, M. Li, H. Geisler, J. Dupire, M. Kerdraon, C. Vergne, F. Monti, *et al.*, "Microfluidic actuators based on temperature-responsive hydrogels," *Microsystems & Nanoengineering*, vol. 4, no. 1, pp. 1–7, 2018.

[30] Y. Koike, Y. Yokoyama, and T. Hayakawa, "Light-driven hydrogel microactuators for on-chip cell manipulations," *Frontiers in Mechanical Engineering*, vol. 6. 2, 2020.

[31] B. Steyrer, B. Busetti, G. Harakály, R. Liska, and J. Stampfl, "Hot lithography vs. room temperature dlp 3d-printing of a dimethacrylate," *Additive Manufacturing*, vol. 21, pp. 209–214, 2018.

[32] N. Tompkins and S. Fraden, "An inexpensive programmable illumination microscope with active feedback," *American journal of physics*, vol. 84, no. 2, pp. 150–158, 2016.

[33] A. Masson, M. Pedrazzani, S. Benrezzak, P. Tchenio, T. Preat, and D. Nutarelli, "Micromirror structured illumination microscope for high-speed in vivo drosophila brain imaging," *Optics express*, vol. 22, no. 2, pp. 1243–1256, 2014.